Melanie Jonasch, Örni Akeret, Aurelio Burgio, Antonio Di Maggio, Morten Harms, Marlen Schlöffel, Steffen Schneider, Dennis Wilken

Selinunte, Italy. A New Model for the City. Field Report on the 2022 to 2023 Seasons

e-Forschungsberichte Faszikel 2 (2024) 1–45 (§)

https://doi.org/10.34780/tbs33n84

Herausgebende Institution / Publisher:
Deutsches Archäologisches Institut

Selinunte, Italy

A New Model for the City

Field Report on the 2022 to 2023 Seasons

MELANIE JONASCH, ÖRNI AKERET, AURELIO BURGIO, ANTONIO DI MAGGIO, MORTEN HARMS, MARLEN SCHLÖFFEL, STEFFEN SCHNEIDER, DENNIS WILKEN

Rome Department of the German Archaeological Institute (DAI)

e-FORSCHUNGSBERICHTE DES DAI **2024** · Faszikel 2

COOPERATION PARTNER

Christian-Albrechts-Universität zu Kiel (D. Wilken); Parco Archeologico di Selinunte, Cave di Cusa e Pantelleria (F. Crescente); Università degli Studi di Palermo (A. Burgio)

FINANCIAL SUPPORT

German Research Foundation

HEAD OF PROJECT

O. Dally, D. Wilken

TEAM

L. Adorno, Ö. Akeret, S. Avitabile, A. Bertaiola, A. Burgio, M. Cangemi, M. Casandra, G. Cassano, G. Contorno, S. Dannemann, S. Debole, N. Di Benedetto, A. Di Maggio, L. Di Rocco, G. Fauci, S. Frey-Kupper, M. Harms, A. Hunkemöller, M. Jonasch, M. La Cecla, C. Lo Cicero, A. Mazzotto, F. Modica, M. Niemöller, F. Pavan, M. Schlöffel, S. Schneider, F. Palumbo, M. Pellittieri, M. Perricone, A. Pullara, A. Reich, A. Romano, A. Rothenheber, S. Rubino, V. Scarpaci, C. Sorce, A. Tortorici, T. Weiler, C. Zarcone

ABSTRACT

This is the second field report of a collaborative project funded by the German Research Foundation in Selinunte, Sicily, since 2021. It aims to enhance our knowledge of the city's layout, its structural transformations through time, as well as its historical, functional, and societal causes. A variety of methods are applied to investigate parts of the city that have until now received less attention. Geophysical prospecting, geological coring, a surface survey, stratigraphic excavations, archaeobotanical analysis, and a wide range of material studies were carried out over three field seasons by the Rome Department of the German Archaeological Institute, the Christian-Albrecht University of Kiel, the University of Palermo, and various collaborators in close consultation with the authorities of the Archaeological Park of Selinunte, Cave di Cusa, and Pantelleria.

KEYWORDS

Urban development, Greek Sicily, Settlement archaeology, Survey, Geophysics, Geoarcheology, Archaeobotany

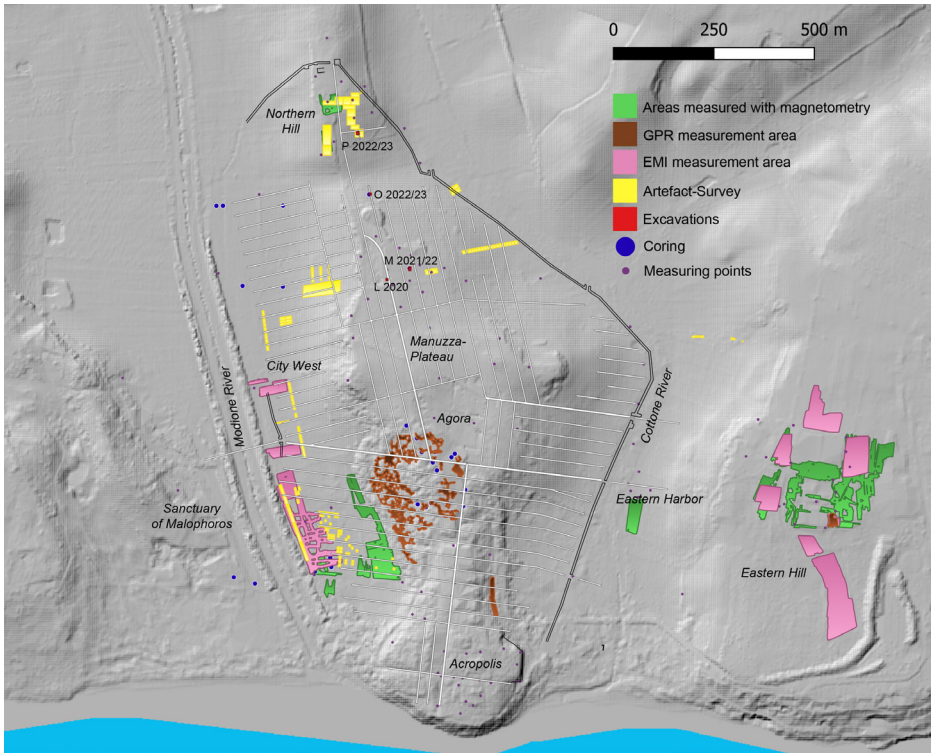

Fig. 1: Overview of the activities carried out as part of the project between 2020 and 2023

ZUSAMMENFASSUNG

Dies ist der zweite Vorbericht über die Feldarbeiten eines Projektes, das seit 2021 im Rahmen einer internationalen Kooperation und gefördert durch die Deutsche Forschungsgemeinschaft in Selinunt, Sizilien, durchgeführt wird. Ziel des Projektes ist die Erweiterung unserer Kenntnisse über den Aufbau der Stadt in ihrer Gesamtheit sowie über die im Laufe der Zeit erfolgten strukturellen Veränderungen und deren historische, funktionale und soziale Ursachen. Mit einer Vielfalt an Methoden wurden vor allem die Bereiche der Stadt in den Blick genommen, die bislang weniger Beachtung in der Forschung fanden. In inzwischen drei Feldkampagnen wurden geophysikalische Prospektionen, Rammkernsondagen, ein Oberflächensurvey, stratigraphische Sondagen, archäobotanische Analysen und eine breite Palette an Materialstudien durch die Abteilung Rom des Deutschen Archäologischen Instituts, die Christian-Albrechts-Universität zu Kiel, die Universität Palermo und verschiedene Mitarbeiter:innen in enger Abstimmung mit den Autoritäten des Archäologischen Parks von Selinunte, Cave di Cusa und Pantelleria durchgeführt.

SCHLAGWÖRTER

Stadtentwicklung, Griechisches Sizilien, Siedlungsarchäologie, Survey, Geowissenschaften, Archäobotanik

Introduction

1 The investigations into the urban fabric and stratigraphy of ancient Selinus (modern Selinunte) largely concern areas of the city hitherto underappreciated by research for various reasons. This applies above all to the urban districts further away from the civic centres, such as the neighbourhoods to the north and west of the central Manuzza plateau.

2 Over three field campaigns, geophysical prospection by the University of Kiel focused respectively on the Eastern Hill, the Modione River valley, and the sand dune between the city's acropolis and agora (Fig. 1, green, pink, and orange areas). There, they tackled fundamental questions such as the overall structure of

Eastern Hill's extra-urban sanctuary, the layout of the central part of town hidden under several metres of sand, and the course of the city's western limits – especially regarding possible harbour facilities. Those efforts, carried out with different geophysical methods, were accompanied by geoarchaeological coring of the sand dune and in the Modione River valley (Fig. 1, blue dots).

3 The surface survey, conducted by the University of Palermo, intended to give an overview of the distribution of surface finds in a chronological and possibly functional perspective. Just as with the geophysical prospections, they focused on areas in the Modione River valley, as well as on the Manuzza Plateau and the Northern Hill (Fig. 1, yellow areas). Due to the heavy compaction of the soil, areas that had undergone some kind of mechanical alteration, such as ploughing, were preferred. The survey was, therefore, carried out partially on agricultural land within the boundaries of the archaeological park.

4 Stratigraphic excavations were conducted on the Manuzza Plateau and the Northern Hill (Fig. 1, red squares). All trenches were positioned within the Greek city of the Archaic and Classical periods but outside the main settlement area of the Hellenistic era. This allowed for the proper investigation of the founding and development of the Greek city, its destruction, and its potential reoccupation with enough precision to document how later inhabitants of the site dealt with the ruin they encountered. In the framework of the excavations, a wide range of material studies was conducted, among which the archaeobotanical analysis is presented here.

5 Preliminary results of the work done so far in the framework of this project have been published in Jonasch et al. 2022, Harms et al. 2023, and Jonasch – Adorno 2024.

Geophysical Prospecting

GPR

6 Ground penetrating radar (GPR) is an active geophysical method for non-invasive prospection of the subsurface. When measuring, the radar device sends short electromagnetic pulses into the ground. The pulses are reflected at electric permittivity contrasts and then recorded at the device. The travel time of the reflection and the speed of electromagnetic waves in solid media can be used to determine the depth of the reflection interfaces. After every transmission, the device records the incoming reflected radar signals for a fixed time, creating a short-time series called trace. Since the radar signals travel from the antenna to the reflector and back, the time until the arrival of a pulse is called two-way time (TWT). The measurement is repeated 30 times per second while the GPR device is moved at a moderate speed along the surface. The traces are visualised in a position relative to the TWT profile. Multiple parallel profiles can be used and interpolated throughout the desired measuring area in order to detect settlement remains. This results in a reflection amplitude data cube that can be cut horizontally into time slices. Such time slices hold the reflection amplitude of a certain travel time interval. If the wave velocity of the area is known, time slices can be transformed into depth slices.

7 Measurements of the sand dune started in 2021. The work done during the first season was presented in Jonasch et al. 2022. Subsequent measurements were begun and completed during two campaigns in 2022 and 2023. Profiles were recorded within the remaining areas of the sand dune accessible for movement (Fig. 1, orange areas). For all measurements, the profiles were randomly walked with an average interval of 30 cm. The GSSI SIR4000 GPR-System with a 400 MHz antenna was used. High-precision positioning was achieved by an RTK differential GPS system (Stonex S9i). Each scan was digitised with 1024 samples/scan. The profiles were interpolated to a constant trace distance of 2 cm, then binned and interpolated into a 3D data cube.

8 Fig. 2 presents an excerpt of the GPR data. The radargram visible in (I) shows the impressive quality of the radar data through the sand of the dune. At shallow depths, the roots of the vegetation can be traced (c). The stratification of the sand dune as well as the hyperbolas of individual stone blocks embedded into the dune, can be identified. Even below the sand dune's base, the signal is not completely attenuated. When interpreting the data, the steep terrain of the sand dune needs to be considered. The resultant radargram's elevation is shown in (II).

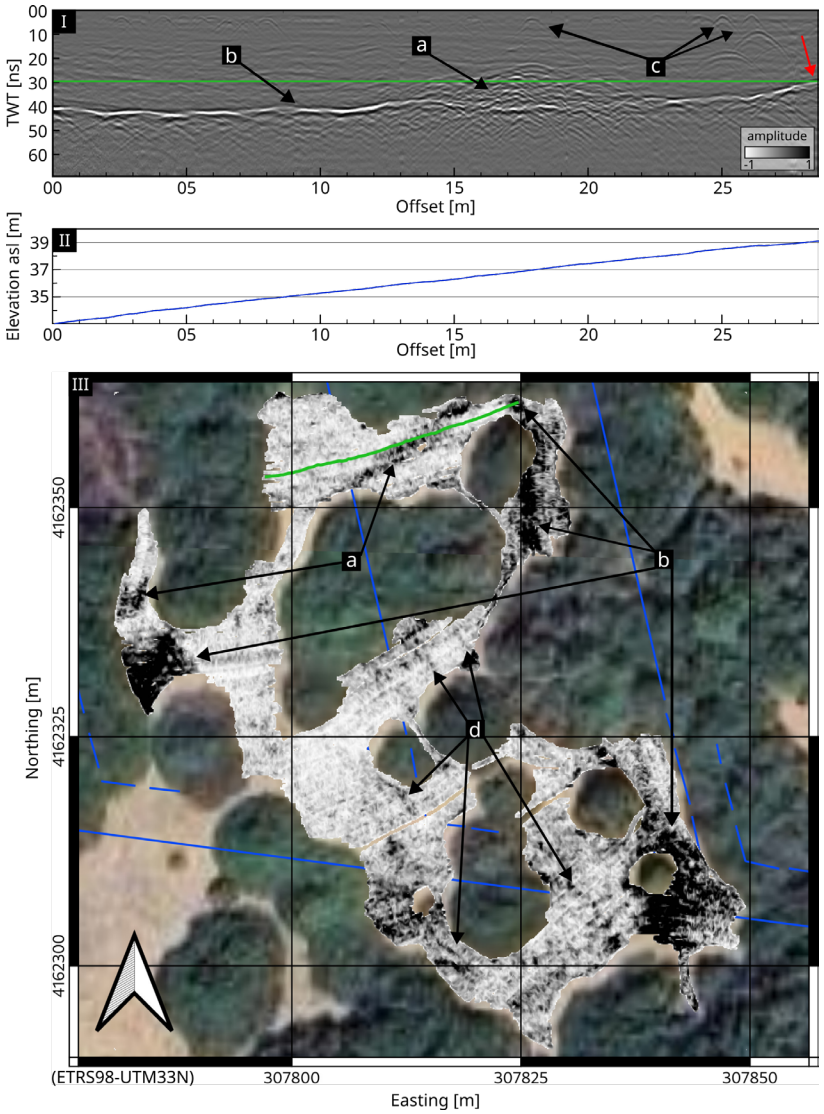

Fig. 2: An example radar data set from the northwestern area of the sand dune: A) shows a time slice at 31 ns into the data cube. The blue markings present the known street layout. The green line depicts the position of Profile 6. The background image is provided by Google; B) The elevation of Profile 6; C) The radargram of Profile 6. The green line depicts the travel time of the time slice shown in A

Meanwhile, Fig. 2 (III) depicts a 2 ns thick slice through the data cube at 31 ns TWT. The blue lines in the background show the extension of known streets and where they supposedly connect. The green line in the radargram (I) marks the depth of the slice shown in (III). The position of the radargram is marked in the slice with a green line as well. Since the slice in (III) is horizontal and flat, it cuts into the horizon at some points. This is marked with a red arrow on the left side of the radargram.

9 The radargram shows the base of the sand dune as a strong reflector, marked with (b). The archaeologically significant features are expected to be in--side or just below this reflector. In the centre of the radargram, a large conglomerate of hyperbolas is marked by (a). This anomaly is likely a collapsed wall. The wall can be traced in the slice (III) for at least 50 m. It is about 5 m wide at its base, similar to sections of the city wall excavated and described by Mertens (2003).

10 As the horizon of the dune base is the strongest reflector in the data, it produces strong anomalies in the slice (III) where it cuts into this horizon. These cuts through the dune‘s base are indicated as (b) in the slice. Several other potential archaeological anomalies are marked with (d) in the slice. These anomalies are elongated and appear anthropogenic, but unfortunately, none of them align with the city’s street layout. It is rather unlikely that the urban planners of Selinus diverted at this point from the orthogonal grid because of the hill’s steep slopes, as no such deviations are observed where slopes are encountered elsewhere in the city.

11 As discussed before, the radar data was recorded in the time domain. To obtain information pertaining to depth, the propagation speed of an electromagnetic wave in the subsurface is needed. A velocity of 0.145 m/ns was estimated by analysing the opening angle of hyperbolas in the dataset. This result conforms to literature values of 0.12–0.17 m/ns for dry sand[1]. With the described velocity, the data cube was 3D depth migrated using a Kirchoff algorithm. Fig. 3 presents the same profile as shown in Fig. 2 but migrated. The data gaps visible in the figure result from the extraction of the profile out of the binned 3D cube after migration.

1 Reynolds 2011.

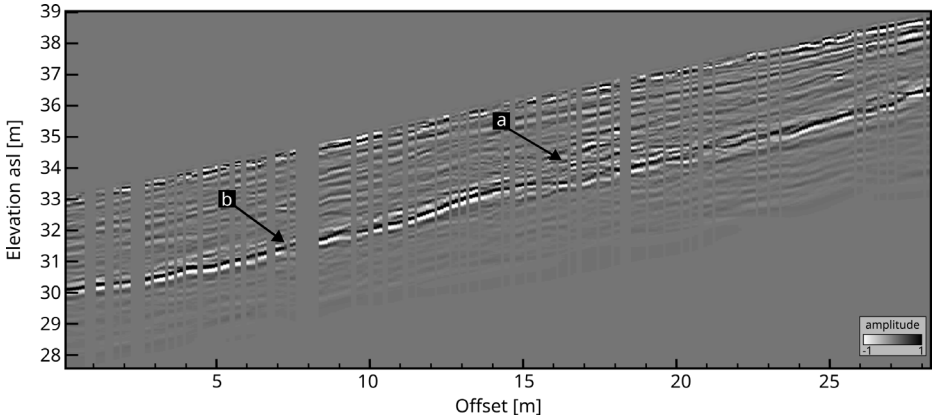

Fig. 3: The radargram of Profile 6 topography and depth migrated. Note the position of Profile 6 can be seen also in Fig. 1

The wall is noted again with (a), and the dune base is marked with (b). The base of the sand dune shows the natural hill on which the Greek settlers built their city. It also becomes evident that the thickness of the dune varies across the area. As expected, it is thicker on the downwind side. At the position of the wall, the dunes base has a 2 to 3-m-long horizontal terrace, functioning as a foundation for the wall. Most of the collapsed sections seem to be resting on the upper slope of the hill, but some of the debris seems to be scattered downhill as well.

12 The horizontal slicing previously cut into the sand dune's base, as illustrated in Fig. 2, created strong disruptive anomalies. As this issue intensifies with the migrated cube, horizontally slicing the cube is not feasible. Unfortunately, picking the horizon by hand is time-consuming and not trivial. Often, the horizon is not as clearly distinguishable as in Fig. 3, and the varying amplitude of the horizon obscures the surrounding anomalies of lower energy. So far, no satisfying way of automating the creation of horizon parallel depth slices has been found in this particular case.

EMI

13 Frequency-domain electromagnetic induction (FDEMI) devices use electromagnetic waves generated in a transmitter and recorded in one or several receiver coils to create maps of electromagnetic subsoil properties at different sensing depths. The transmitter coil emits a ›primary‹ harmonic oscillating electromagnetic wavefield (kHz frequency range). This field induces eddy currents in the subsoil that depend on the electrical conductivity of the soil. These oscillating eddy currents generate a ›secondary‹ field, which, in superposition with the primary field, is recorded at the receiver coils. Based on this, the EMI method measures the apparent electrical conductivity of the soil and the so-called in-phase property, which is a function of the magnetic susceptibility. The penetration depth of the EMI method depends not only on the device configuration, namely the signal frequency, the transmitter-receiver distance and orientation, and the measurement height above ground, but also on the soil properties themselves.

14 During the 2022 Selinunte campaign, the GF Instruments CMD Mini-Explorer EMI device was employed (Fig. 1, pink areas). It is composed of one

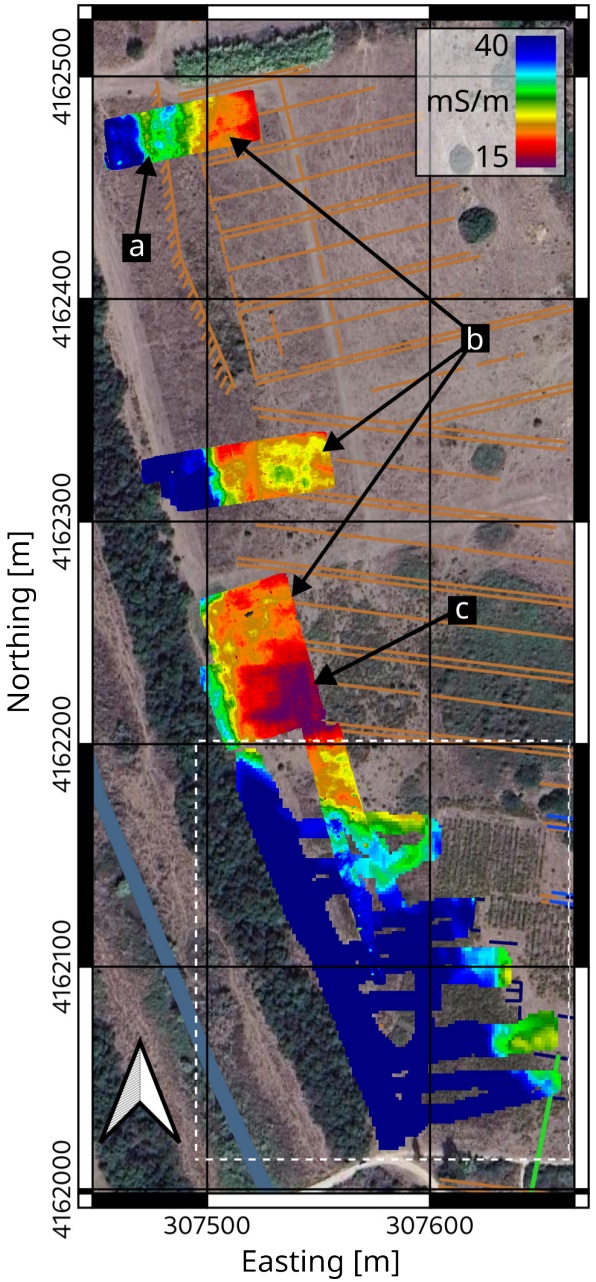

Fig. 4: The EMI data recorded in the Modione River valley. The apparent conductivity of the second coil pair is presented. Brown and blue notations represent the known street layout. The background image is provided by Google

transmitting coil and three receiving coils. The coils were used horizontally in a coplanar orientation (HCP). The measured EC is an integral along the response curve. The response curve shows a distinct maximum at a depth corresponding to the inter-coil distance. Therefore, effective depths of 0.5, 1.0, and 1.8 m can be assigned to the three inter-coil-distances. The output consists of three apparent electric conductivity (ECa) maps corresponding to the three depths. The data was recorded at a normal walking speed with a sampling rate of 10 Hz. High-precision lateral positioning was achieved using an RTK-GPS device (Stonex S9i). Close to 37,000 m² were recorded across four measurement areas in the Modione River valley and nine areas at the Eastern Hill. The areas were covered by randomly walked west-to-east oriented profiles with an average spacing of 0.5 m.

15 The EMI data of each profile was processed separately. The GPS positions were corrected for the centre of each coil pair. The EMI data was corrected for the device time drift. A spatial bandpass filter was applied with cutoff frequencies of 0.0001 (1/sample) and 0.2 (1/sample). The data was gridded at an increment of 0.25 m. The gridded map was smoothed with a 0.5 m half-width Gaussian image filter.

16 Fig. 4 presents EMI data from the Modione River valley. The figure shows the measurements of the second coil pair corresponding to a depth of 1 m. For comparison, the known street layout is drawn in the background of the figure. Only a 130 m long section of the city wall had been found in this valley[2]. The anomaly marked with (a) is 5 m west of the previously known city wall, yet it is the only anomaly that conforms to a wall. The wall anomaly visible in the first EMI area is not found in the other measurement areas. Linear structures can be determined in all EMI areas. The structures of low conductivity aligned with the street layout are indicated by (b). The structures are inside different insulae and are interpreted as structural walls. The materials with higher conductivity in between the walls are probably fluvial sediments accumulated in the ruins through inundation events. The remnants of a rectangular building of at least 30 × 30 m are indicated by (c). The building does not align with the orthogonal layout of the Greek city.

2 Mertens 2003.

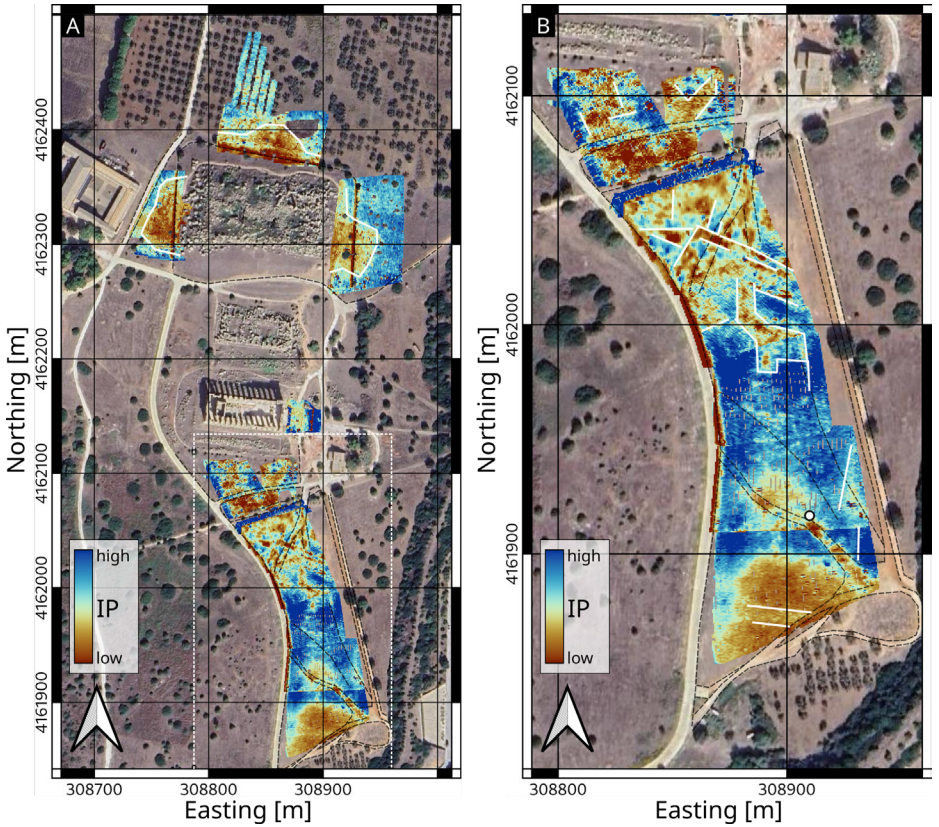

Fig. 5: The IP component of the EMI data. The maps in A) are all set to the same colour map. The maps in B) are individually scaled to highlight features. The position of B) is marked by a dashed white square in A). The dashed black lines trace recent streets. The anomalies are marked by smooth white lines. The white dot shows the position of the pictures in Fig. 6. The background image is provided by Google

This suggests a later usage. A survey described in Jonasch et al. 2022 notes an accumulation of late Roman pottery sherds in this region[3]. Therefore, it could be interpreted as a Roman farm or warehouse close to the river.

17 The area indicated within the dashed white rectangle was recorded differently from the previous EMI area. Here, the vegetation prevented the measurement of the sort of tightly spaced profiles necessary to create high-resolution maps. Instead, separate randomly walked profiles between the bushes were recorded. The profiles have been interpolated to 4 m to facilitate the viewing. In this area, it is not possible to discuss individual structures but rather the overall geology of the river valley. In a river context, high conductivity, seen in blue here, is associated with fine sediments like silt or clay. The first two EMI areas show a distinct drop in ECa at the onset of the built-up area. This is not the case for the EMI area inside the dashed lines. Here, the high ECa area reaches into the built-up area. The sediment cores in Fig. 9 and 10 show that the archaeological layer becomes thinner close to the river. The fluvial sediments located closer to the surface likely produced the high ECa. The sediment core 42 is situated where the EMI map has a slightly lower ECa (green). Here, the archaeological layer is almost twice as thick compared to the cores 26 and 27, made closer to the river.

18 For the EMI measurement of the Eastern Hill, instead of apparent electric conductivity (ECa), the in-phase (IP) component of the EMI data was drawn on for interpretation because it shows several peculiar features. The IP maps for the third coil pair are presented in Fig. 5A. Dashed black lines trace modern roads' positions on the satellite image. The roads appear in the IP maps and obscure the interpretation (Fig. 5B is an excerpt at the position of the dashed white line in A). Anomalies on each side appear as if the debris of the temple is spread out over a greater area underground. It might also indicate a calcarenite limestone outcropping through the topsoil. The broad and loosely defined features south of Temple E similarly appear to be geologic in nature (Fig. 5A). The calcarenite, described by Piro and Versino (1995), is thickest below the temples and decreases southwards. Meanwhile, Fig. 5B illustrates several elongated anomalies visible in the central

3 See also A. Burgio and A. Di Maggio below.

Fig. 6: Outcropping bedrock on the Eastern Hill. The position of the outcrop is marked by a white dot in Fig. 5. The tape measure is not aligned with the structure

sector. Unfortunately, none of these features are aligned with either the temples or the city's street layout. These elongated anomalies could be understood as cuttings into the calcarenite limestone bedrock to create level foundations for structures. The southernmost anomaly, marked with two parallel white lines, appears to form a straight passage 6 m wide cut into the bedrock. While taking measurements in the field, rocky outcroppings were observed at several places on the Eastern Hill, some of which featured carvings or shaping into rectangular forms that appeared to be anthropogenic in origin (Fig. 6).

M. Harms, D. Wilken

Geoarchaeological Investigations

19 A geoarchaeological study campaign complemented the geophysical prospection in the western region of Selinunte's urban zone. They aimed at uncovering the stratigraphic setting of the Modione River valley in general, particularly at the transition from the ancient urban area to the river's floodplain. Geological soundings and the analysis of sediments and archaeological layers comprised these investigations. The same methodology was employed for the investigation of the sand dune north of the city's acropolis in 2021[4]. The information obtained helps to compare, validate, and interpret the geophysical data.

20 During ten days of fieldwork in September 2022, 18 sediment cores were retrieved from the lower western neighbourhoods of the city and the Modione River valley (Fig. 1, blue dots). The majority of the corings lie within the bounds of the geophysical prospection areas (Figs. 7). Hollow metal probes (diameter: 5 cm; length: 100 cm) were driven into the ground with a petrol breaker (Atlas Copco TT, Fig. 8) and extracted with a hydraulic device. Unlike extensive archaeological excavation, these precise corings have a minimal impact on the archaeological site. They are nearly non-destructive and can be carried out quickly.

4 Jonasch et al. 2022.

Fig. 7: Overview of the corings in the Modione River valley

21 The results of the geoarchaeological investigations of sediments and archaeological layers are presented below using the stratigraphic sections A and B as examples (Figs. 9 and 10). The sections have a north-south orientation and run parallel to the artificially embanked channel of the Modione. Stratigraphic Section A (corings 26, 27, and 31) covers the deepest parts of the floodplain near the watercourse. Stratigraphic Section B (corings 28, 32, 38, 42, and 45) lies ca. 40 m east and represents the transition to the more elevated areas of the valley floor.

22 The cores were examined according to pedological, sedimentological, and archaeological features. As macroscopic features are often not sufficient to reliably determine the origin and formation of a layer, samples from select core sections were analysed for microscopic scale components[5]. By wet sieving, different fractions between 2 mm and 100 µm were extracted from the samples. They were analysed using a stereomicroscope at up to 45-× magnification with a special focus on the identification of plant, animal, and anthropogenic remains.

23 Up to 7 m below the surface, transects A and B show three major stratigraphic units: the recent topsoil (I), archaeological layers (II), and natural sediments (III). The recent topsoil (I) is well mixed, has a high organic content, and is mostly fine-grained. It contains an abundance of anthropogenic components dating from ancient times to the modern era. Among them are sherds, glass fragments, burnt clay, and charred plant remains. The topsoil has developed in a substrate that we assume consists of a mixture of overbank deposits from the Modione, slope deposits from the western slope of the hill on which the ancient city stands, and reworked cultural layers. There are clear indications that the effects of modern agricultural use, especially ploughing, extend to a depth of 45 to 95 cm below the modern surface.

24 The archaeological layers (II) below the topsoil contain a high quantity of artifacts that point to ancient settlement activities. Among them are fragments of pottery, roof tiles, clumps of burnt clay, stone and stone packs, bone fragments,

5 Albers et al. in prep.

Fig. 8: Fieldwork in the Modione River valley

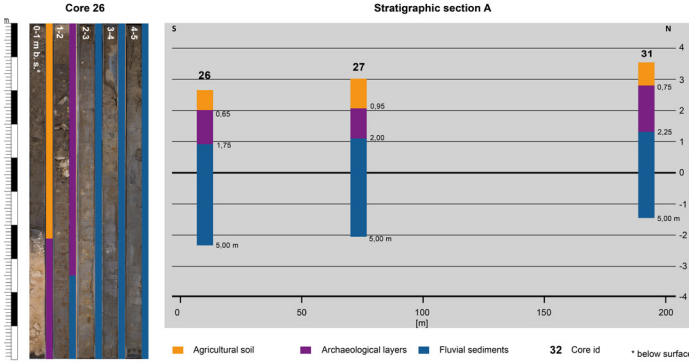

Fig. 9: The stratigraphic section A crosses the valley bottom near the recent Modione channel. The photo of core 26 is representative of the stratigraphic section A

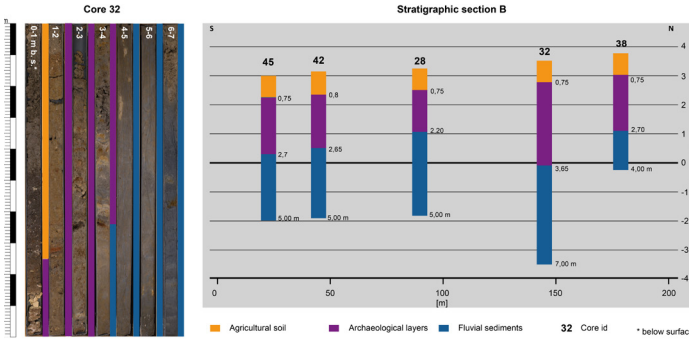

Fig. 10: The stratigraphic section B, crossing the farm in the lower valley from the recent Modione channel. The photo of core 32 is representative of the stratigraphic section B

and charcoal. The second meter of core 45, for example, contains the nose of an ancient oil lamp. The composition of the archaeological layers is heterogeneous and chaotic. Grain size, colour, and organic content vary irregularly. No layer is continuously traceable in all profiles. At the current state of research, we are not able to differentiate between *in situ* cultural layers and reworked or redeposited layers.

25 The thicknesses of the archaeological layers vary from a minimum of ca. 1 m (cores 26 and 27) to a maximum of ca. 2.9 m (core 32). The height above modern sea level (asl) of the base of the archaeological layers also deviates considerably, laying approximately between 1 m asl and 0.1 m below sea level. It appears that the surface of the ancient landscape was significantly more accentuated than today. The reason for this has yet to be investigated. Possible causes are irregularities in the natural topography prior to colonisation, anthropogenic interventions, and/or erosional processes.

26 In both transects A and B, the archaeological layers lie on top of natural overbank deposits (III). The sediments do not contain any anthropogenic indicators and have a sandy-silty, mostly homogeneous, matrix. In the third meter below the surface, some sandy layers occur. In the fourth meter below the surface, approximately at today's sea level, a change from sandy-silt to silty-clayey material occurs. It is accompanied by an increase in the organic content and the occurrence of snail shell fragments. The microscopic analysis of the material gives no evidence of a marine or lagoonal environment as existed at the time in the Cotone Valley, where ostracods and foraminifers indicate a saline environment[6]. Accordingly, we interpret the sediments of the third stratigraphic unit as fluvial deposits within the floodplain of the Modione.

M. Schlöffel, S. Schneider

6 Albers et al. in prep.

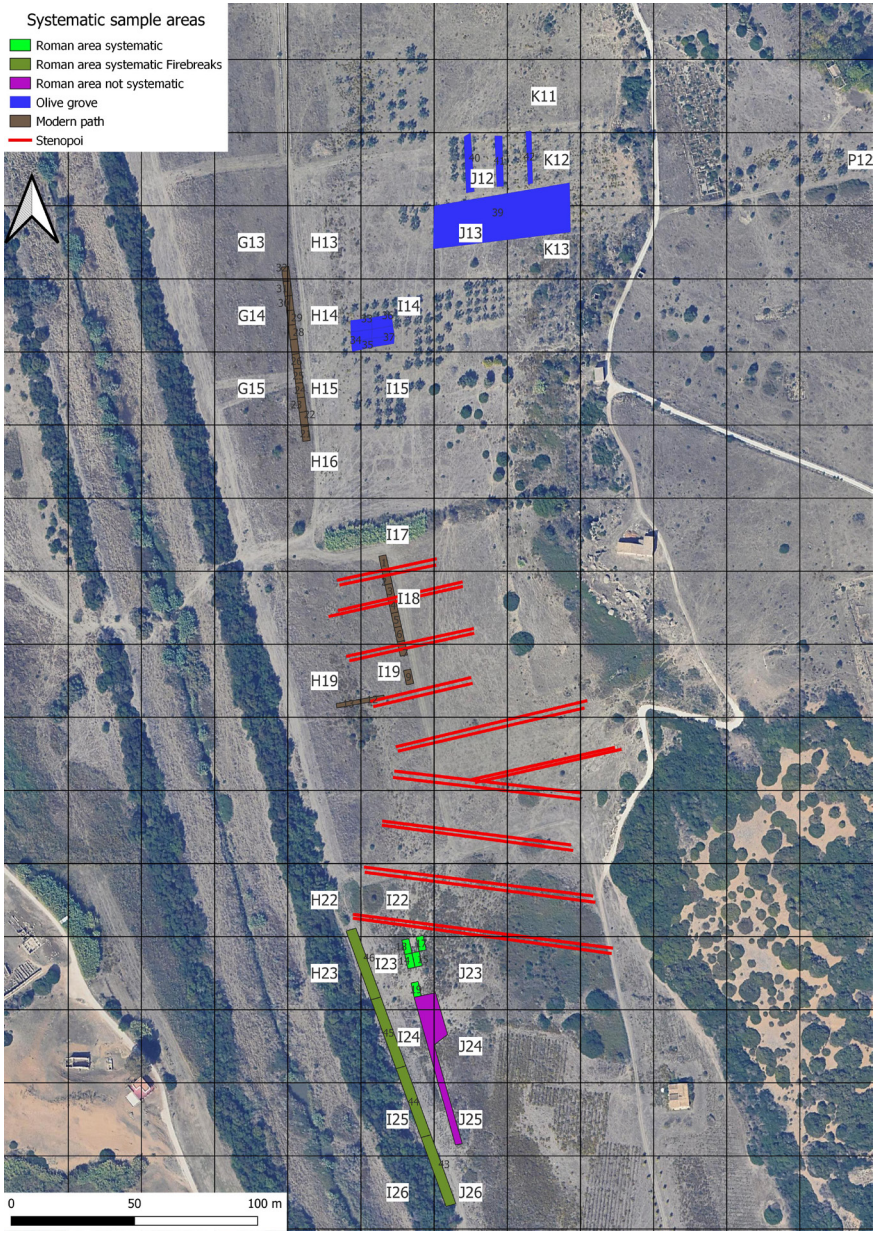

Fig. 11: Systematic sampling in the western area of Selinunt

Surface Survey

27 The study here presented is the continuation of the survey initiated in 2021 and was carried out in 2022 and 2023 as part of a curricular laboratory for students at the University of Palermo (Bachelor's in Cultural Heritage and Master's degree in Archaeology). The basis for the systematic recording of the finds was once again the virtual grid of 50 × 50 m (quadrants) laid out in 2021 across the entire area of the park (Fig. 1). Within these quadrants, smaller plots or transects were selected for surveying, based on reasons of topography and visibility. All surface finds were identified and counted while diagnostic sherds and unusual finds were collected. Previously unmodified surfaces could also be raked superficially to check for differences in density and quality of finds (i. e., shovel-test sampling).

28 In 2022, the survey was carried out in the western district of the Modione River valley, where three sectors were investigated. One in the south (Fig. 11, green and fuchsia) was selected to better define the extension of an area where, in 2021, comparatively high quantities of Roman pottery were found[7]. The analytical choice was also guided by the anomalies detected both by aerial photography and by the geophysical investigations[8]. This preliminary information allowed us to diversify the survey methodology by collecting in smaller plots, larger transects, or even in loosely defined areas. Both transects investigated in this first sector were 50 m long and 5 or 7 m wide (Fig. 11, light and dark green). An area of approximately 800 m² inside the quadrants I23–24 and J23–25 was not divided into plots or transects because its low visibility did not allow for the systematic counting of surface finds, but only random sampling (Fig. 11, fuchsia). In quadrant I23, 10 % of the area was investigated by systematic sampling, the average density being around 11.7 fragments per m². With a density of 23.4 fragments per m², transect Q14 clearly stands out from the average. The classes of finds (which properly will be published elsewhere) were as follows: *amphorae* 33 %, coarse ware 30 %, roof tiles 22 %, fine tableware 11 %, *pithoi* 4 %, millstones < 1 %, lamps < 1 %. The ratio within the single transects was similar, except for transect Q18, which had a higher amount of fine tableware.

7 Jonasch et al. 2022, 65.
8 See above D. Wilken and M. Harms.

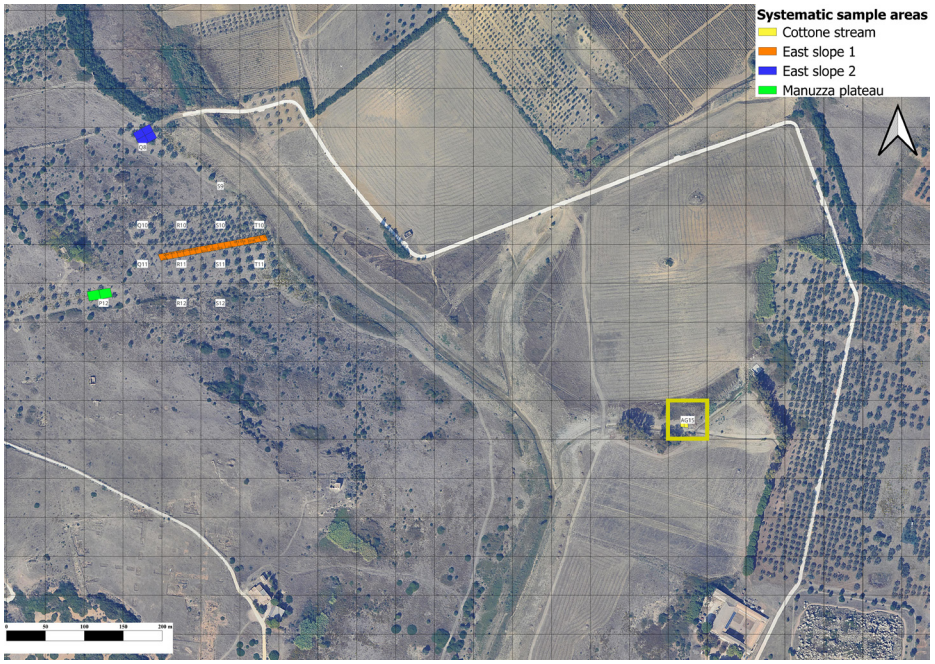

Fig. 12: Systematic sampling on the Manuzza plateau and in the Cottone River valley

29 The second sector was located about 100 m further north (Fig. 11, brown). Eight plots with a dimension of 50 m² were investigated either after mowing or after mechanically disturbing the surface. The plots are all located within the quadrants I17–19 and the neighbouring H19. In this sector, the density level varies significantly: in I18, where 10 % of the total was sampled, the average density of finds was 4.7 fragments per m²; in quadrant I19 (with 6 % coverage), the density drops to 2.5 fragments per m²; in quadrant H19 (2 % coverage) the density is 3.2 fragments per m². Finally, the most northerly plot located in I17 revealed a density of only 0.36 fragments per m².

30 Some 50 m further north, another series of 50 m² plots were studied inside the quadrants H14, 15, 16, and G3. As in the preceding plots, mowing and shovel tests were carried out to increase the quantity of the surface finds. The density remained, however, very low, with around 0.6 fragments per m². This could be due to the presence of a thick alluvial or arable soil covering cultural layers attested in the plots to the south or because of a low use frequency of the area in antiquity.

31 A little to the east, an olive grove was comparatively examined thoroughly with a coverage of 24 % (Fig. 11, blue). Despite the ploughed ground, the density of the findings remained rather low: around one fragment per m², with many *pithoi* among the sampled material.

32 In 2023, the survey included areas on the Manuzza plateau covered in olive groves (Fig. 12, green). They were chosen for visibility since they were freshly ploughed. The systematic sampling was carried out using the disposition of the olive trees as a lead (Fig. 13). The first plots measured about 365 m² and were located at a short distance from Trench M, excavated earlier as part of this overarching project[9]. The density of finds within these plots was 3.1 fragments per m². The classes of finds – *amphorae* 5 %, coarse ware 44 %, roof tiles 39 %, fine tableware 10 %, *pithoi* 2 %, millstones < 1 %, lamps < 1 % – did not provide any further information. The second sector investigated was located along the eastern slope of the Manuzza plateau (Fig. 12, orange). A transect of about 1210 m² was selected for sampling after carrying out a preliminary investigation in the area. The average density turned out to be 2.3 fragments per m², but the distribution was not uniform.

9 Jonasch – Adorno 2024.

Fig. 13: Systematic sampling on the Manuzza plateau: pottery sampling in the olive groves (= Fig. 12, green)

The highest density was in the plots located at lower elevations at 5.47 fragments per m^2 over an area of 177.6 m^2. It is reasonable to assume that this is due to natural erosion. It could, however, also indicate an increased use of this area at the point of transition to the Cottone Valley below. Also, in this area, the find typologies – *amphorae* 2 %, coarse ware 37 %, roof tiles 43 %, fine tableware 2 %, *pithoi* 16 %, millstones < 1 %, lamps < 1 %, flint < 1 % – do not provide any further information.

33 Finally, a survey was carried out outside the city walls and east of the Cottone River, which was subject to cleaning measures in Spring 2023 (Fig. 12, yellow). As a small inlet from the river was freed from dense vegetation, a larger quantity of pottery appeared along wide sections of the freshly cleaned banks. The finds show a wide chronological range, dating from the 5th century BCE to the Late Roman and even Early Medieval periods. During the survey, two walls, made from blocks of marl and mortar, were also cleaned and documented. At the moment, it is difficult to fully understand the purpose of this area through the ages since the selective intervention alongside the waterways left the surrounding areas hidden under dense vegetation.

34 In terms of chronology, it can be predicted that the rather few diagnostic finds made in all the described sectors will fall well within the well-known phases of the city's life. More precise data will be available after the thorough examination of the finds is completed.

A. Burgio, A. Di Maggio

Stratigraphic Excavations

35 The excavation of Trench M on the Manuzza plateau was completed in 2022, with preliminary results having recently been published[10]. The same year, two new trenches were opened on the northern slope of Manuzza and on the southern slope of the Northern Hill (Fig. 1, red squares). The goal of these trenches was to obtain an overview of the stratigraphic sequence in these parts of the ancient city, which have so far been unexplored through excavation. In terms of

10 Jonasch – Adorno 2024.

Fig. 14: Trench O with street and post-antique building

Fig. 15: Trench O, southern section from inside the post-antique building

site development, the geomagnetic prospection carried out in the area of these trenches in the early 2000s proved to be inconclusive[11].

36 Trench O 2022/23 opened along the north slope of the Manuzza, measured 5 per 5 m, and contained a street with a north-south orientation, flanked by a massive wall composed of reused stones of varying type and size (Fig. 14). Together with two smaller east-west orientated walls built exclusively of quarried stone, this large wall enclosed an area 4 m in length but of an unknown depth. Although the ceramics on the street and within the building were exclusively pre-Roman, the stratigraphy and disordered masonry of the main wall suggest a dating of the building in the medieval period. Surprisingly, it was not possible to find any preceding structures underneath. Within and under the walls of this late building, we only found a massive layer of sterile yellow clay with lime inclusions (Fig. 15). After following this layer for about 80 cm, the decision was made to discontinue excavations in this area. A core sample taken next to the trench also contained only about 70 cm of topsoil and possible archaeological layers above silty natural deposits. This observation raises the question of whether parts of the northern slope of the Manuzza plateau might have been devoid of buildings in ancient times and used instead for varying purposes like clay extraction or other types of production.

37 Trench P 2022/23 was also initially laid out as a 5 by 5 m square but was subsequently enlarged to allow the excavation of an entire room of about 23 m^2 (see Fig. 19). The corner room of a single-storey private building is flanked by two streets on its northern and eastern sides. Within the walls of quarried stone and mud brick, it was possible to uncover an almost completely collapsed roof consisting of pan and cover tiles (Fig. 16). The collapse probably occurred during the Carthaginian attack in 409 BCE, as the objects discovered underneath the roof were shattered *in situ* by the impact rather than being cleared away or looted. An overturned louterion was lying on the badly preserved clay floor with a coin from Akragas nearby, dating between 415 and 406 BCE (Fig. 17. 18). A large number of finds were retrieved from under the roof collapse, including about 12 *amphorae*, multiple cooking pots and various kitchenware, black-glazed fine wares, as well as miniature vessels and terracotta figurines. All dateable material corresponds to the

11 Mertens 2003.

Fig. 16: Montage of orthophotos of the collapsed roof in room 1

Fig. 17: Trench P, detail of the crushed inventory with tipped-over louterion. To the right of the vessel a tetras from Akragas

Fig. 18: Louterion after provisional restauration

Fig. 19: Trench P, final state of excavation

second half of the 5th century BCE. In the northern part of the room, two fireplaces were found, built from reused roof tiles in one instance and stones in the other. Both bear distinct burn marks and can be interpreted as hearths (Fig. 19). On the western hearth, remains of a cooking grate were still in situ. Since the collapse of the roof also contained two pierced tiles, it is possible that those were placed on the roof to allow smoke from these hearths to disperse. The room was obviously used for preparing meals. It had three doors that opened to two adjacent rooms in the west and one in the south. The state of conservation there was similar, especially in the western rooms. The trench was nevertheless not further enlarged. The information gathered from the excavated area already allows the rare possibility of reconstructing a nearly complete inventory of a 5th-century kitchen or a multifunctional space also used for cooking.

38 Earlier phases of use were mainly found in the southern part of the trench, where older walls served as foundations for the 5th-century building. Due to the limited space, it was not possible to define the form and function of these preceding features. It was, however, interesting to learn that the street along the eastern side of the room was developed only in the last phase of use. Underneath the street layers were strata attesting to different activities, sadly indefinable over such a small area.

M. Jonasch

Archaeobotanical Investigations

39 During a ten-day study in June 2023, a series of soil samples were processed for archaeobotanical analyses. The wash-over method was used, which has proven to be particularly gentle[12]. As transport capacities were limited, a simplified flotation device was used. The sieve mesh sizes were 4, 1, and 0.35 mm. In order to save water in arid Sicily, a system was developed that reused the water: the water was collected in a tank below the sieves and pumped up into a barrel using a wastewater pump (Fig. 20). From there, the filtered water flowed back down the

12 Steiner et al. 2015.

Fig. 20: Simplified flotation system with water recycling

	Bronze age	~600–550 BCE	~400–300 BCE
number of US analysed	2	6	1
total volume (litres)	10.3	63.2	5.4
cultivated plants			
Cerealia (Getreide/cereali) – charred grain	.	14	2
Ficus carica (Feige/fico) – mineralised fruit	.	5	.
Ficus carica (Feige/fico) – charred fruit	.	.	1
Hordeum vulgare (Gerste/orzo) – charred grain	.	21	.
Triticum aestivum/durum/turgidum (Nacktweizen/frumento) – charred grain	.	2	.
Triticum monococcum (Einkorn/farro piccolo) – charred grain	.	1	.
Triticum spec. (Weizen/frumento) – charred grain	.	1	.
Vitis vinifera (Weintraube/vite) – charred seed	.	1	1
cultivated or wild plants			
Avena spec. (Hafer/avena) – charred awn	.	22	.
Fabaceae (Hülsenfrüchte/legume) – charred seed	.	1	.
Vicieae (Wickenähnliche Hülsenfrüchte/fabacee simili alla veccia) – charred seed	1	2	.
wild plants			
Apiaceae (Doldenblütler/ombrellifere) – charred fruit	.	2	.
cf. *Chaenorhinum* (Kleines Leinkraut?/linaiola?) – charred seed	23	5	2
Chenopodiastrum murale (Mauer-Gänsefuss/chenopodio murale) – charrded seed	.	.	1
Lolium cf. *temulentum* (Taumel-Lolch?/loglio ubriacante?) – charred fruit	.	5	.
Lysimachia spec. (Gauchheil/Gilbweiderich/centocchio) – charred seed	.	4	.
Malvaceae (Malvengewächse/malvacee) – charred seed	.	5	.
cf. *Medicago* (Schneckenklee?/erba medica?) – charred seed	.	2	.
Phalaris spec. (Glanzgras/phalaris) – charred seed	1	11	2
Plantago spec. (Wegerich/piantaggine) – charred sed	.	2	2
Poaceae (Süssgräser/graminacee) – charred fruit	1	10	3
Poaceae (Süssgräser/graminacee) – charred awn	4	2	.
Poaceae (Süssgräser/graminacee) – charred rachis segment	.	2	.
Polygonaceae (Knöterichgewächse/poligonacee) – charred fruit	.	1	.
Rumex spec. (Ampfer/romice) – charred fruit	.	1	1
Selaginella denticulata (Gezähnter Moosfarn/selaginella denticolata) – mineralised megaspore	.	1	.
Triticum neglectum/vagans (Vernachlässigter/eiförmiger Walch/cerere comune/ginocchiata) – charred fruit	.	1	.
Valerianella spec. (Ackersalat/gallinella) – mineralised fruit	.	1	.

Fig. 21: Table of plant finds

slope to the sieves. The system proved to be efficient; comparatively little water had to be added.

40 Most of the material analysed dates from the 6th century BCE; two samples were from the Bronze Age, and one was between 400 and 300 BCE[13]. The samples analysed were selected in close consultation with the excavators. In the first step, different contexts were tested. Further sediment samples were prepared from those that proved positive. In total, 78.9 l of sediment were processed.

41 The organic fractions were analysed using a stereomicroscope (magnification 6.5 ×–40 ×). Identification of plant remains was done using scholarly literature[14] and a modern seed reference collection, including material collected in the archaeological park.

42 The quantity of discovered plant remains is rather low. That said, compared with similarly dated sites from southwest Sicily, they are above average[15]. With one exception, all samples yielded seeds and fruits. A total of 170 identifiable plant remains were counted, of which 163 were charred, and seven were preserved in mineralised form (Fig. 21). Charring is an incomplete combustion process. As the use of fire was common in all archaeological periods, this is generally the most frequent form of preservation. The prerequisite for mineralisation is a high concentration of phosphate, which is usually found in latrines or dung heaps. The presence of mineralised remains in the excavation structures raises questions, as these buildings were evidently not used as stables or latrines. It is more likely that these deposits were mixed with sediments from earlier or later utilisation.

43 Forty-nine of the findings are cultivated plants; a further 26 findings are possibly cultivated plants. Among the cereals, barley is by far the most prominent (Fig. 22), although naked wheat and einkorn wheat were also identified. The oat awns could also come from one of the wild species common in the Mediterranean region. Two fruit species have been identified with the finds of grape and fig seeds. The few legume seeds were too poorly preserved to be clearly identified. All of the

13 Jonasch – Adorno 2024.
14 E. g. Sabato – Peña-Chocarro 2021.
15 Moricca et al. 2021; Stika et al. 2008.

Fig. 22: Charred barley grain (Hordeum vulgare)

Fig. 23: Charred fruit of glossy grass (Phalaris spec.)

crop species identified may have originated from local cultivation and did not have to be imported.

44 The dominance of barley contrasts with earlier investigations from Selinunte, where naked wheat dominated[16]. Naked wheat was also predominant at the Phoenician-Punic site of Motya[17]. It remains to be analysed whether this difference has chronological causes or is related to the function of the structures from which these samples were taken. Most cultivated plants were found in the clay hearth. This is where we find the clearest evidence of food preparation and household use. No cultivated plants were found at all in the two Bronze Age samples or in a fill of a rubbish pit of the early 6th century that mainly contained ashes. This may be due to the fact that if the temperatures during combustion are too high and there is a strong supply of oxygen, plant remains burn completely and are not preserved[18].

45 The wild plant spectrum still needs to be analysed in greater detail. A preliminary analysis suggests that arable weeds are mainly found in samples with a lot of cereals. For example, glossy grass (*Phalaris* spec.) is one of the most frequently found taxa (Fig. 23). One species from this genus – *Phalaris coerulescens* – still grows today as a weed in the cereal fields of the archaeological park.

Ö. Akeret

16 Stika et al. 2008.
17 Moricca et al. 2021.
18 Berihuete-Azorín et al. 2019.

References

Albers et al. in prep. J. Albers – A. Miß – C. Haubenthal – A. Pint – H. Renners – M. Rimböck – M. Schlöffel – S. Schneider – B. Weissová, Der Osthafen von Selinunt. Zwischenbericht zu den Feldforschungen im Tal des Gorgo Cotone 2019 – 2021, Römische Mitteilungen, in preparation

Berihuete-Azorín et al. 2019 M. Berihuete-Azorín – H.-P. Stika – A. Bourliva – L. Papadopoulou – S.-M. Valamoti, »Fresh from the Oven«: Experiments on Triticum Spelta and a Protocol for Carbonising Specimens for Archaeobotanical Comparison Collections, JASc 26, 2019, 101865, https://doi.org/10.1016/j.jasrep.2019.05.030

Harms et al. 2023 M. Harms – D. Wilken – M. Jonasch – E. Corradini – E. Erkul – W. Rabbel, Starting to Fill the Gaps of the Selinus Geophysical Map. Advances in On- and Offshore Archaeological Prospection Proceedings of the 15th International Conference on Archaeological Prospection, Kiel University Publishing, 711–720, https://doi.org/10.38072/978-3-928794-83-1/p72

Jonasch – Adorno 2024 M. Jonasch – L. Adorno, Un Altro Saggio della Stratigrafia del Pianoro di Manuzza. Rapporto Preliminare, FOLD&R 581, 2024, https://www.fastionline.org/docs/FOLDER-it-2024-581.pdf

Jonasch et al. 2022 M. Jonasch – L. Adorno – A. Burgio – A. Di Maggio – M. Harms – M. Schlöffel – S. Schneider – D. Wilken, Selinunt, Italien. Forschungen in Selinunt, Teil 1. Ein neues Modell für die Stadt Selinunt. Die Feldarbeiten des Jahres 2021, eDAI-F 2022-1, § 1–33, https://doi.org/10.34780/ftd4-fm24

Mertens 2003 D. Mertens, Selinus I, 2. Die Stadt und ihre Mauern. Beilagen (Mainz 2003)

Moricca et al. 2021 C. Moricca – L. Nigro – L. Masci – S. Pasta – F. Cappella – F. Spagnoli – L. Sadori, Cultural Landscape and Plant Use at the Phoenician Site of Motya (Western Sicily, Italy) Inferred from a Disposal Pit, Vegetation History and Archaeobotany 30, 2021, 815–829, https://doi.org/10.1007/s00334-021-00834-1

Piro – Versino 1995 S. Piro – L. Versino, Geological Survey in the Archaeological Area of Selinunte, Annals of Geophysics 38(5–6), 1995, 893–906, https://doi.org/10.4401/ag-4093

Reynolds 2011 J. M. Reynolds, An Introduction to Applied and Environmental Geophysics ²(Oxford 2011)

Sabato – Peña-Chocarro 2021 D. Sabato – L. Peña-Chocarro, Maris Nostri Novus Atlas. Seeds and Fruits from the Mediterranean Basin. MaNNA Project (Madrid 2021)

Steiner et al. 2015 B. L. Steiner – F. Antolín – S. Jacomet, Testing of the Consistency of the Sieving (Wash-Over) Process of Waterlogged Sediments by Multiple Operators, JASc 2, 2015, 310–320, https://doi.org/10.1016/j.jasrep.2015.02.012

Stika et al. 2008 H.-P. Stika – A. G. Heiss – B. Zach, Plant Remains from the Early Iron Age in Western Sicily: Differences in Subsistence Strategies of Greek and Elymian Sites, Vegetation History and Archaeobotany 17, 2008, 139–148, https://doi.org/10.1007/s00334-008-0171-9

IILLUSTRATION CREDITS

Fig. 1: DAI Rom, Melanie Jonasch
Fig. 2: Morten Harms
Fig. 3: Morten Harms
Fig. 4: Dennis Wilken, Morten Harms
Fig. 5: Dennis Wilken, Morten Harms
Fig. 6: Dennis Wilken, Morten Harms
Fig. 7: Steffen Schneider
Fig. 8: Malin Niemöller
Fig. 9: Steffen Schneider, Marlen Schlöffel
Fig. 10: Steffen Schneider, Marlen Schlöffel
Fig. 11: Antonio Di Maggio
Fig. 12: Antonio Di Maggio
Fig. 13: Aurelio Burgio
Fig. 14: DAI Rom, Melanie Jonasch
Fig. 15: DAI Rom, Melanie Jonasch
Fig. 16: DAI Rom, Melanie Jonasch
Fig. 17: DAI Rom, Melanie Jonasch
Fig. 18: DAI Rom, Daniela Gauss
Fig. 19: DAI Rom, Melanie Jonasch
Fig. 20: Örni Akeret
Fig. 21: Örni Akeret
Fig. 22: Örni Akeret
Fig. 23: Örni Akeret

CONTACT

Dr. Melanie Jonasch
Deutsches Archäologisches Institut, Abteilung Rom
Via Sardegna 179-181
00187 Rom
Italy
melanie.jonasch@dainst.de
ORCID-iD: https://orcid.org/0000-0001-6144-4017
ROR ID: https://ror.org/023md1f53

Dr. Örni Akeret
Universität Basel
Bernoullistrasse 30
4056 Basel
Switzerland
oerni.akeret@unibas.ch
ORCID-iD: https://orcid.org/0000-0002-5057-9255
ROR: https://ror.org/02s6k3f65

Prof. Dr. Aurelio Burgio
Università degli Studi di Palermo
Viale delle Scienze, Ed. 15
90128 Palermo
Italy
aurelio.burgio@unipa.it
ORCID-iD: https://orcid.org/0000-0002-8679-0335
ROR: https://ror.org/044k9ta02

Dr. Antonio Di Maggio
Università degli Studi di Palermo
Viale delle Scienze, Ed. 15
90128 Palermo
Italy
ORCID-iD: https://orcid.org/0000-0003-3348-1763
ROR: https://ror.org/044k9ta02

Morten Harms, M. Sc.
Christian-Albrechts-Universität zu Kiel, Institut für Geowissenschaften
Otto-Hahn-Platz 1
24118 Kiel
Germany
morten.harms@ifg.uni-kiel.de
ORCID-iD: https://orcid.org/0000-0002-1446-0193
ROR: https://ror.org/04v76ef78

Dr. Marlen Schlöffel
Enreco GbR, Büro für Geoarchäologie und Bodenkunde Schneider & Schlöffel
Leipziger Straße 24b
75181 Pforzheim
Germany
m.schloeffel@enreco.de
ORCID-iD: https://orcid.org/0000-0002-9417-8760

Dr. Steffen Schneider
Enreco GbR, Büro für Geoarchäologie und Bodenkunde Schneider & Schlöffel
Leipziger Straße 24b
75181 Pforzheim
Germany
schneider@enreco.de
ORCID-iD: https://orcid.org/0000-0001-9728-4107

Dr. Dennis Wilken
Christian-Albrechts-Universität zu Kiel, Institut für Geowissenschaften
Otto-Hahn-Platz 1
24118 Kiel
Germany

dennis.wilken@ifg.uni-kiel.de
ORCID-iD: https://orcid.org/0000-0002-5128-351X
ROR: https://ror.org/04v76ef78

METADATA

Titel/*Title*: Selinunte, Italy. A New Model for the City. Field Report on the 2022 to 2023 Seasons

Band/*Issue*: e-Forschungsberichte 2024-2

Bitte zitieren Sie diesen Beitrag folgenderweise/*Please cite the article as follows*: M. Jonasch – Ö. Akeret – A. Burgio – A. Di Maggio – M. Harms – M. Schlöffel – S. Schneider – D. Wilken, Selinunte, Italy. A New Model for the City. Field Report on the 2022 to 2023 Seasons, eDAI-F 2024-2, § 1–45, https://doi.org/10.34780/tbs33n84

Online veröffentlicht am/*Online published on*: 19.12.2024

DOI: https://doi.org/10.34780/tbs33n84

Schlagworte/*Keywords*: Urban development, Greek Sicily, Settlement archaeology, Survey, Geophysics, Geoarcheology, Archaeobotany

Bibliographischer Datensatz/*Bibliographic reference*: https://zenon.dainst.org/Record/003083366